AEMR

Advances in Energy and Materials Research

https://jaem.qom.ac.ir/

Enhanced Adsorption of Cd(II) and Pb(II) Using Amine-Modified MCM-41 Mesoporous Silica

Samira Rasouli

Department of Chemistry, Faculty of Science, Imam Khomeini International University, Qazvin, Islamic Republic of Iran.
Email: chemmj94@gmail.com

Article Info

Article type:
Research Article

Article history:
Received 12 Feb 2024
Received in revised form 29 May 2024
Accepted 24 Jul 2024
Published online 28 Sep 2024

Keywords:
Mesoporous silica, Amine modification, Heavy metal removal, Adsorption kinetics, Isotherm modeling.

ABSTRACT

This research investigates the synthesis and characterization of MCM-41 molecular sieves functionalized with 3-aminopropyltriethoxysilane (APTES) to evaluate their efficacy in adsorbing heavy metal ions, such as Cd(II) and Pb(II), from aqueous solutions. Amine-modified MCM-41 samples with 3, 5, 8, and 15 wt% APTES were synthesized via a co-condensation method using cetyltrimethylammonium bromide (CTAB) as the template, APTES for functionalization, and tetraethyl orthosilicate (TEOS) as the silica precursor. The adsorbents were characterized using X-ray diffraction (XRD), nitrogen adsorption-desorption isotherms (BET), thermogravimetric analysis (TG-DTG), Fourier-transform infrared spectroscopy (FT-IR), and transmission electron microscopy (TEM). Batch adsorption experiments assessed the effects of initial metal ion concentration, solution pH, adsorbent dosage, and temperature. All NH2-MCM-41 variants exhibited higher adsorption capacities for Cd(II) and Pb(II) than unmodified MCM-41, with performance varying by amine loading. The enhanced adsorption was attributed to amine groups on the pore surfaces and external surfaces of the mesoporous silica. For the optimized adsorbent (5 wt% NH2-MCM-41), maximum adsorption efficiencies were 89.1% for Cd(II) at pH 5.0–6.0 and 95.3% for Pb(II) at pH 3.0–3.5, with precipitation effects considered negligible under these conditions. Adsorption isotherms conformed to the Langmuir model, indicating monolayer adsorption. Kinetic studies revealed that adsorption followed the pseudo-second-order model for both Cd(II) and Pb(II).

Cite this article: Rasouli, S., (2025). Enhanced adsorption of cd(ii) and pb(ii) using amine-modified mcm-41 mesoporous silica, *Advances in Energy and Materials Research*, 2 (1), 40-54. https://doi.org/10.22091/jaem.2025.13195.1027

DOI: 10.22091/jaem.2025.13195.1027

Publisher: University of Qom.

1. Introduction

Heavy metals, defined by densities exceeding 5 g/cm³ and significant toxicity [1], pose a major environmental challenge due to industrial activities such as chemical production (e.g., paints, coatings, tanneries, fertilizers) and mining. Contamination of water resources with heavy metals is a critical issue, as their bioaccumulative and non-biodegradable nature leads to persistent accumulation, adversely affecting human health and ecosystems. Lead, cadmium, copper, mercury, chromium, nickel, and zinc are among the most hazardous heavy metals in wastewater, causing various health disorders due to their toxicity and accumulation in living tissues and the food chain [2].

Cadmium is used in alloy production, metal plating, mining, and ceramics and is a contaminant in phosphate fertilizers, detergents, oils, photocells, and refined petroleum products [3]. Chronic exposure to cadmium is linked to kidney dysfunction, respiratory issues (e.g., lung cancer), hepatic toxicity, and bone disorders such as osteomalacia and osteoporosis [4].

Lead contamination arises from textile dyeing, petroleum refining, ceramics, glass manufacturing, battery production, and mining [5]. High exposure levels cause neurological impairments, developmental delays, and cognitive damage by compromising the blood-brain barrier [6]. Lead also induces oxidative stress, leading to kidney dysfunction, reproductive issues, and symptoms such as anemia, insomnia, headaches, and dizziness [7, 8]. Consequently, cadmium and lead levels in wastewater exceeding World Health Organization (WHO) guidelines pose significant public health and environmental risks.

Various techniques, including chemical precipitation, ion exchange, membrane separation, filtration, and reverse osmosis, have been explored for heavy metal removal [9-13]. While effective, these methods often face challenges such as high costs or limited metal recovery. Adsorption is widely recognized as a practical, efficient, and cost-effective water treatment strategy [14], offering flexible designs and the potential for high-purity effluent. In some cases, adsorption allows regeneration via desorption.

Numerous adsorbent materials—such as silica [15, 16], clay [17], activated carbon [18], titania [19, 20], and synthetic resins [21]—have been studied for heavy metal removal. Although activated carbon is effective, alternative adsorbents are being developed to improve efficiency at low contaminant concentrations. Hybrid organic-inorganic mesoporous materials have emerged as promising adsorbents. Amine-functionalized adsorbents offer high surface area, strong metal ion affinity via coordination bonds, and potential for regeneration [22]. Studies have demonstrated heavy metal adsorption using amine-modified mesoporous silica [24], which feature high surface area, uniform pores, and large pore volume [25, 26], with modifiable silica frameworks [27].

Organic functionalization of mesoporous silica can be achieved via grafting [28] or co-condensation [29]. Grafting attaches organosilanes to silanol groups, but may reduce pore size, cause uneven coverage, and block pores, decreasing efficiency at high amine loadings [30]. Co-condensation incorporates functional groups uniformly during synthesis, preserving the mesoporous structure, though high organic loadings may disrupt ordering [31, 32].

This study synthesizes amine-functionalized MCM-41 (NH2-MCM-41) via co-condensation for efficient cadmium and lead ion removal from aqueous solutions. Amine functionalization with 3-aminopropyltriethoxysilane (APTES) enhances metal ion coordination. The study evaluates adsorption parameters, including initial metal ion concentration, solution pH, adsorbent dosage, and temperature, and analyzes isotherms and kinetics to elucidate the adsorption mechanism.

1. Experimental

1.1 Materials

All materials and solvents were purchased from reputable companies without further purification.

1.1.1. Preparation of Standard Solutions

Stock solutions of cadmium and lead at a concentration of 1000 ppm were prepared by separately dissolving cadmium chloride (2.54 g) and lead nitrate (2.48 g) in

1000 cm³ of deionized water. Subsequently, a series of standard solutions with cadmium and lead concentrations of 5, 10, 20, 30, 40, and 50 ppm were obtained by stepwise dilution of their respective stock solutions.

1.1.2. Preparation of NH_2-MCM-41: Amine Functionalization through Co-Condensation Approach

The synthesis of NH_2-MCM-41 followed a reported literature method [33]. Initially, a mixture containing cetyltrimethylammonium bromide (CTAB, 2.0 g, 5.5 mmol), ammonium hydroxide solution (205 mL, 5320 mmol), and water (270 cm³) was heated at 50°C for 30 minutes, maintaining a pH of 12.4. Once a homogeneous solution was obtained, tetraethyl orthosilicate (TEOS, 10 cm³, 45 mmol) and APTES (3 cm³, 13 mmol) were added sequentially. A white precipitate began forming within three minutes of stirring. The reaction temperature was then held at 50°C for six hours to complete the synthesis.

The precipitate obtained was separated using filtration, thoroughly washed with deionized water and ethanol, and subsequently dried under vacuum at ambient temperature. To remove the surfactant incorporated during synthesis, a solvent extraction procedure was employed. Specifically, 1.0 g of the material was subjected to reflux for six hours in a solution comprising 1 mL of concentrated HCl (37%) and 100 mL of ethanol. The sample was then washed multiple times (three cycles) with ethanol and deionized water to ensure complete purification. Finally, the NH_2-MCM-41 adsorbent was isolated via filtration and dried under vacuum for 24 hours.

To modify the amine content, APTES was varied across different concentrations, including 3 mL (13 mmol), 5 cm³ (21 mmol), 8 cm³ (34 mmol), and 15 cm³ (64 mmol). Consequently, amine-functionalized MCM-41 samples with varying weight percentages were synthesized and labeled as 3 mL-NH_2-MCM-41, 5 mL-NH_2-MCM-41, 8 mL-NH_2-MCM-41, and 15 mL-NH_2-MCM-41, respectively.

1.2. Characterization

1.2.1. Powder X-ray Diffraction (PXRD)

The structural arrangement of the synthesized materials was examined using low-angle XRD analysis. The diffraction patterns were obtained with a Philips PANalytical X'pert PRO MPD Diffractometer, utilizing Cu Kα radiation (λ = 0.15406 nm). A divergence slit of 5 mm was employed, with data acquisition carried out in increments of 0.02° and a time step of 10 s, covering the angular range of $0.5° < 2θ < 10°$.

1.2.2. N2 Adsorption-Desorption Isotherms

To determine the surface area of the synthesized adsorbents, nitrogen adsorption-desorption experiments were conducted at 77 K using a Micromeritics Tristar 3000 analyzer. Before testing, samples were subjected to a two-step degassing procedure: an initial treatment at 90°C for 2 hours followed by extended heating at 250°C for 6 hours to ensure complete removal of residual moisture and solvents. The relative pressure (P/Po) was systematically increased from 0 to 1. The specific surface area (SBET) was calculated using the Brunauer–Emmett–Teller (BET) equation. Additionally, total pore volume (VT) was estimated based on nitrogen uptake at $P/Po \approx 0.99$, while pore size distribution was analyzed using the Barrett–Joyner–Halenda (BJH) method.

1.2.3. Transmission Electron Microscopy (TEM)

To assess the morphology of the amine-functionalized MCM-41 samples, transmission electron microscopy (TEM) was performed using a Philips EM430 electron microscope set at an accelerating voltage of 200 kV. Sample preparation involved grinding the materials into fine particles, dispersing them in ethanol, and subjecting the mixture to ultrasonication for 15 minutes. A small volume of the resulting dispersion was carefully deposited onto a copper grid and left to air-dry before imaging.

1.2.4. Thermal and Differential Thermogravimetric Analysis (TGA-DTG)

The thermal stability of the synthesized adsorbents was examined using TG/DTG analysis under nonisothermal conditions, employing a TA Instruments Q600 SDT simultaneous TGA-DSC analyzer. The experiments were conducted across a temperature range of 30–800°C, with a controlled heating rate of 10°C/min. Sample weights were kept between 5–10 mg, and the analysis was performed under a nitrogen atmosphere, maintaining a flow rate of 10 cm^3/min.

1.2.5. Fourier Transform Infrared (FTIR) Spectroscopy

Functional groups present in the synthesized materials were characterized via infrared spectroscopy within the range of 4000–600 cm^{-1}. The analyses were performed on a Bruker Tensor 27 spectrometer equipped with a Pike ATR attachment, and the spectral data was processed using OPUS software.

1.2.6. Elemental Analysis (EA)

Elemental composition, specifically CHN analysis, was conducted utilizing an Elementar Vario Micro Cube instrument integrated with a thermal conductivity detector (TCD).

1.2.7. Batch Adsorption Studies

Adsorption experiments were performed under ambient conditions (20±2°C) using a Stuart SSL2 reciprocal shaker set to an agitation speed of 250 min^{-1}. For each test, 0.100 g of adsorbent was introduced into 20 mL of aqueous solutions containing either Cd(II) or Pb(II) ions, with the suspensions being continuously stirred for 2 hours to reach equilibrium. The samples were then centrifuged at 1000 rpm for 15 minutes, and the supernatant was separated using a 0.22 µm syringe filter. The residual concentrations of Cd(II) and Pb(II) ions in the filtrates were subsequently quantified via atomic absorption spectrophotometry (AAS).

1.2.8. Influence of pH on Adsorption

The effect of pH on adsorption was explored across different ranges: 2.0–6.0 for Cd(II) and 2.0–5.0 for Pb(II). Beyond pH 6.0, lead ions rapidly precipitated, restricting further studies [34]. Solution pH values were adjusted using 0.1 M NaOH or 0.1 M HCl solutions. A fixed quantity of adsorbent (0.100 g) was added to metal solutions (25 cm^3) containing various metal ion concentrations (5–50 ppm) and agitated at room temperature for 2 hours.

1.2.9. Effect of Initial Metal Ion Concentration

The influence of metal ion concentration was examined at pH 6.0 for Cd(II) and pH 5.0 for Pb(II), varying the concentrations of metal ions in solution. The centrifuged supernatants were analyzed to determine final metal ion concentrations. Experiments were conducted in duplicate, with reported results representing mean values.

1.2.10. Adsorbent Dosage

The role of adsorbent dosage was evaluated by varying the amount from 0.25 to 3.0 g in a 20 cm^3 solution containing 20 ppm of metal ions (Cd(II) or Pb(II)) at optimal pH conditions. After 2 hours of agitation, the solutions were centrifuged and filtered, with final metal ion concentrations analyzed via atomic absorption spectroscopy.

1.2.11. Effect of Temperature

Adsorption behavior at different temperatures (20, 30, 40, and 50°C) was studied using 0.2 g of 5 mL-NH_2-MCM-41 adsorbent in a 30 ppm metal ion solution. pH values were maintained at 5.5 for Cd(II) and 3.0 for Pb(II), with samples agitated for 2 hours at each specified temperature.

1.2.12. Adsorption Models

Two adsorption models were employed to interpret experimental data:

1) Langmuir Model (Equation 3) [35]**:** This model assumes monolayer adsorption onto a surface with uniform adsorption sites. It is represented in its linearized form:

Ceqe=1qmaxb+Ceqmax\frac{C_e}{q_e} = \frac{1}{q_{\text{max}} b} + \frac{C_e}{q_{\text{max}}}

where qeq_e is the equilibrium adsorption capacity (mg/g), CeC_e is the equilibrium concentration (mg/L), qmaxq_{\text{max}} denotes the maximum adsorption capacity (mg/g), and bb is the Langmuir constant.

2) Freundlich Model (Equation 4) [36]: This empirical model describes multilayer adsorption on heterogeneous surfaces:

qe=KfCe1nq_e = K_f C_e^{\frac{1}{n}}

where qeq_e represents the equilibrium adsorption capacity (mg/g), CeC_e is the equilibrium concentration (mg/L), KfK_f is the Freundlich constant related to adsorption capacity, and nn is the adsorption intensity factor.

Experimental adsorption data were fitted to these models in Microsoft Excel, with R-squared values used to assess the best-fitting model.

2. Results and Discussion

2.1. Adsorbent Characterization

XRD analysis revealed characteristic diffraction peaks indicative of the ordered hexagonal mesoporous structure of MCM-41, with a prominent d100 reflection appearing at $2\theta \approx 2.41°$, alongside lower intensity peaks corresponding to d110, d200, and d210 planes. Amine-functionalized samples exhibited a slight shift in the d100 peak, reflecting structural modifications due to APTES incorporation. Increasing the APTES content (from 13 to 64 mmol) led to a gradual reduction in peak intensity and resolution, a trend similarly reported by Toshiyuki et al. [37]. TEM images further confirmed the retention of a one-dimensional pore structure, though with reduced ordering compared to pure MCM-41.

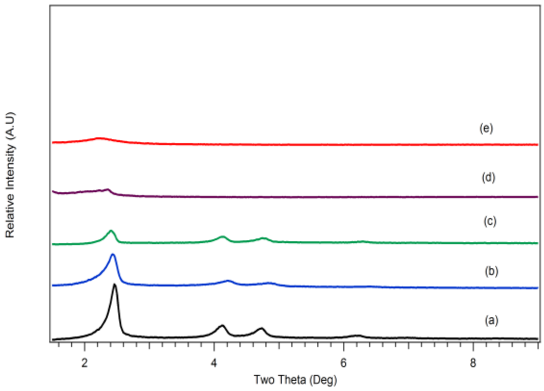

Figure 1. The X-ray diffraction profiles correspond to the following samples: (a) unmodified MCM-41, (b) NH_2-MCM-41 synthesized with 3 mL of amine precursor, (c) NH_2-MCM-41 containing 5 mL of amine precursor, (d) NH_2-MCM-41 incorporating 8 mL of amine precursor, and (e) NH_2-MCM-41 modified with 15 mL of amine precursor.

Gas adsorption and desorption on the clean surfaces of dry powdered solids is a widely adopted method for determining the surface area of adsorbents. During these experiments, the material undergoes heating while being degassed using either a vacuum or an inert gas like nitrogen to eliminate any previously adsorbed substances. Nitrogen adsorption-desorption analysis was carried out to examine how different levels of amine functionalization impact the specific surface area and pore size of the modified MCM-41 samples. The N_2 adsorption isotherms of both unmodified and amine-functionalized samples are illustrated in Fig. 2a, while Fig. 2b presents their respective pore size distribution curves. All samples exhibited type IV isotherms, which are characteristic of mesoporous materials. The slope observed within the intermediate range of relative pressure (P/Po = 0.30–0.70) signifies capillary condensation of nitrogen within the mesopores, whereas the type H1 hysteresis loop at P/Po < 0.9 is indicative of interparticle macroporosity.

Table 1 provides details regarding specific surface areas and pore sizes of adsorbents, both before and after amine functionalization. As the amount of amine loading increased, noticeable reductions in surface area, pore size, and pore volume were observed in amine-modified MCM-41 samples when compared to the unfunctionalized MCM-41. The surface area and pore size of pure MCM-41 were measured at 1306 m^2 and 3.20 nm, respectively, but after amine modification, these values dropped to 740 m^2 and 1.80 nm. In Fig. 2a, the first capillary step occurs at a relative pressure of P/Po = 0.37, though after amine functionalization, it shifts to a lower partial pressure and becomes more broadly distributed. Additionally, capillary condensation in the amine-modified samples is observed over a wider P/Po range relative to pure MCM-41, indicating a less uniform pore size distribution and reduced pore volume, as reflected in Table 1.

It is important to note that introducing 3-aminopropyltriethoxysilane to the mesoporous MCM-41 framework significantly reduces its surface area, pore size, and pore volume due to the presence of amino groups on the structure. Similar findings were previously reported by Jin-Heong Yim et al. [38], confirming that functionalization alters the physicochemical properties of the material.

Table 2 presents the elemental analysis results, demonstrating that approximately 90% of the aminopropyl groups from APTES were successfully incorporated into the MCM-41 framework. This high functionalization efficiency further validates the modification process.

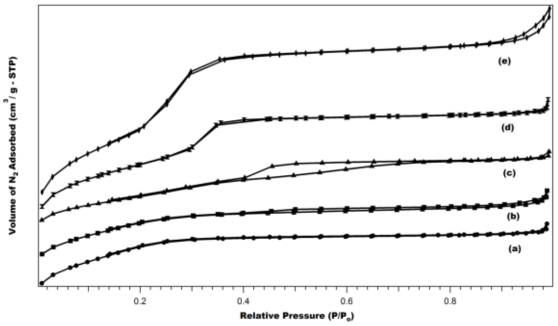

Figure 2a. Nitrogen adsorption-desorption isotherm profiles for both unmodified MCM-41 and amine-functionalized variants.

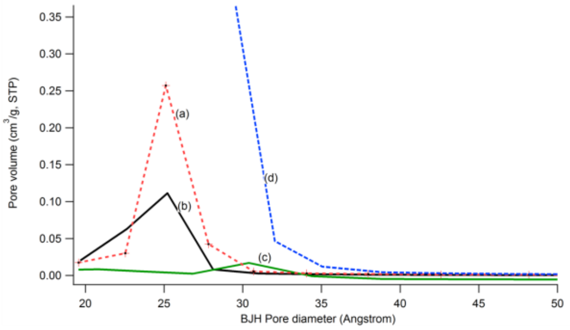

Figure 2b. Pore size distribution graphs corresponding to the following samples: (a) unmodified MCM-41, (b) NH_2-MCM-41 with 3 mL of amine precursor, (c) NH_2-MCM-41 incorporating 5 mL of amine precursor, (d) NH_2-MCM-41 modified with 8 mL of amine precursor, and (e) NH_2-MCM-41 containing 15 mL of amine precursor (not s

Table 1. Textural Properties of Pure and Amine-Functionalized MCM-41 Adsorbents

Sample	SBET (m²/g)	VT (cm³/g)	Dp (nm)	d100 (nm)	a₀ (nm)	Wwall (nm)
Pure MCM-41	1306	1.03	3.20	3.84	4.52	1.32
3 mL-NH₂-MCM-41	1115	0.99	2.83	3.55	4.18	1.35
5 mL-NH₂-MCM-41	996	0.84	2.50	3.92	4.61	2.11
8 mL-NH₂-MCM-41	802	0.65	2.40	4.17	4.90	2.50
15 mL-NH₂-MCM-41	740	0.57	1.80	4.39	5.10	3.30

V_T: The total pore volume is determined based on the amount of nitrogen adsorbed at a relative pressure (P/Po) of approximately 0.95. The pore diameter (Dp) is assessed using the adsorption segment of the isotherms, while the wall thickness (twall) is calculated by subtracting the pore size from the overall structural dimensions.

Table 2. Sample Analysis: Nitrogen Content and Incorporation Efficiency

Sample	Theoretical N Content (mmol/g)	Actual N Content via EA (mmol/g)	Incorporation Efficiency (%)
3 mL-NH₂-MCM-41	0.39	0.36	92
5 mL-NH₂-MCM-41	0.64	0.61	95
8 mL-NH₂-MCM-41	1.30	1.10	85
15 mL-NH₂-MCM-41	1.93	1.67	86

To investigate the nature and distribution of functional groups on the aminopropyl-functionalized silica surface, Fourier-transform infrared (FTIR) spectroscopy was employed. Figure 3 illustrates the FT-IR spectra of both modified and unmodified mesoporous MCM-41 samples. As shown in Fig. 3a, the unmodified MCM-41 exhibits characteristic absorption bands at 1051, 805, and 556 cm^{-1}, which correspond to the stretching vibrations of the silica network (Si-O-Si). Additionally, the bending vibration associated with adsorbed water molecules (H-O-H) appears within the spectral range of 1620–1640 cm^{-1}.

In comparison, the amine-functionalized samples reveal two additional absorption bands—one at 691 cm^{-1}, attributed to Si-C stretching vibrations, and another at 1468 cm^{-1}, corresponding to asymmetric C-N stretching [40]. These peaks stem from the –Si-$(CH_2)_3$-NH_2 groups introduced via APTES modification. The emergence of N-H bending vibrations at 691 cm^{-1} and symmetric -NH_2 bending vibrations at 1468 cm^{-1}, which are absent in pure MCM-41, signifies the successful incorporation of amine groups onto the pore surfaces.

All spectra contain a broad band in the region of 3100–3400 cm^{-1}, which can be assigned to ν(O-H) vibrations of adsorbed water molecules. Furthermore, amine-modified samples (NH_2-Si-MCM-41) exhibit distinct asymmetric stretching vibrations corresponding to the -CH_2 groups of the propyl chain at 2921 cm^{-1} and 2852 cm^{-1} (marked with arrows) [41]. These features, absent from pure MCM-41, confirm the effective grafting of the amine functionality onto the material's surface.

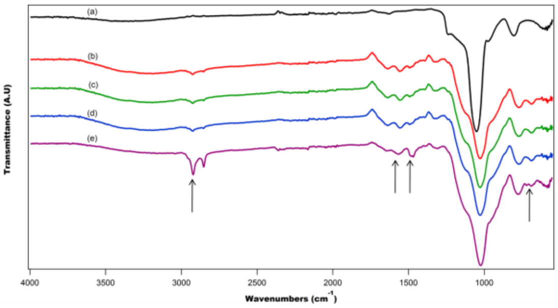

Figure 3. FT-IR spectral profiles corresponding to the following samples: (a) unmodified MCM-41, (b) NH_2-MCM-41 synthesized with 3 mL of amine precursor, (c) NH_2-MCM-41 containing 5 mL of amine precursor, (d) NH_2-MCM-41 incorporating 8 mL of amine precursor, and (e) NH_2-MCM-41 modified with 15 mL of amine precursor.

Fig. 4a and 4b present TEM images of both unmodified MCM-41 and an amine-functionalized MCM-41 sample. The pristine MCM-41 exhibits well-defined parallel channels, characteristic of its hexagonal pore arrangement. In contrast, the amine-modified samples display a less distinct hexagonal structure, suggesting that functionalization has partially altered the mesoporous framework. These observations align with the XRD findings, which indicate a reduction in peak intensity and the disappearance of certain diffraction signals. This suggests that the originally uniform small mesopores were partially occupied by the incorporated organic amine groups.

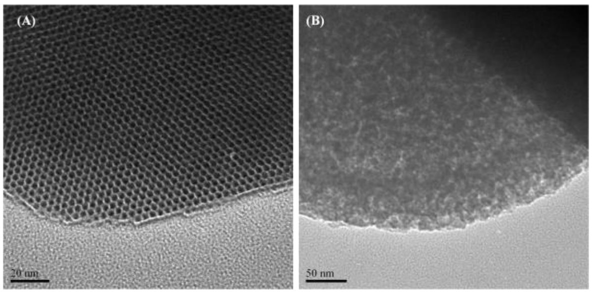

Figure 4. TEM Analysis of Mesoporous Silica and Functionalized Adsorbent (a) Transmission electron micrograph of MCM-41 and (b) TEM image of 5 mL-NH_2-MCM-41, highlighting morphological differences**.**

The thermal gravimetric (TG) and differential thermogravimetric (DTG) analysis results for pure MCM-41, 5 mL-NH_2-MCM-41, and 15 mL-NH_2-MCM-41 are depicted in Fig. 5. In the case of the unmodified sample, an initial mass reduction of approximately 15% below 100°C is attributed to the removal of physically adsorbed water molecules.

The TG profiles of the amine-functionalized materials, specifically 5 mL-NH_2-MCM-41 and 15 mL-NH_2-MCM-41, exhibit three distinct weight loss stages, as evidenced in the DTG curves (Fig. 5b). The first stage, observed at temperatures below 100°C, corresponds to the desorption of physisorbed moisture. The second mass loss phase, occurring between 210–390°C, is associated with the thermal decomposition of amine groups attached to the mesoporous silica walls [42]. The third and final stage, beyond 400°C, is linked to the combustion of residual carbon-containing species [43].

Comparative thermal stability assessments reveal that pure MCM-41 undergoes a 15% weight loss when heated from 30 to 800°C, whereas the functionalized samples exhibit greater mass reductions—30% for 5 mL-NH_2-MCM-41 and 34% for 15 mL-NH_2-MCM-41. The more pronounced weight loss in the 15 mL-NH_2-MCM-41 sample compared to its 5 mL counterpart signifies the presence of a higher concentration of amine groups in the structure. These findings confirm the successful incorporation of amine functionalities onto the MCM-41 framework, demonstrating high thermal stability up to approximately 350°C.

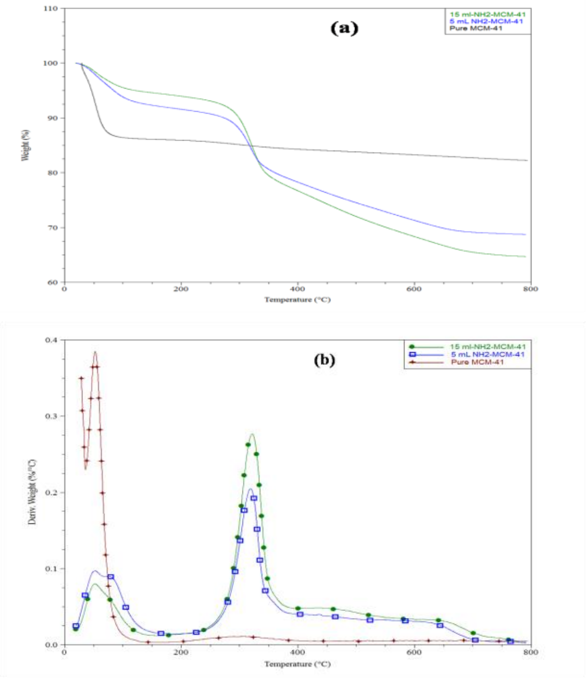

Figure 5. Thermal Analysis of MCM-41 and Amine-Functionalized Adsorbents (a) Thermogravimetric analysis (TGA) and (b) derivative thermogravimetry (DTG) profiles for pure MCM-41, 5 mL-NH_2-MCM-41, and 15 mL-NH_2-MCM-41 adsorbents.

2.2. Adsorption Behavior of Cd(II) and Pb(II) Ions on NH_2-MCM-41 Adsorbent

Figure 6 illustrates the adsorption performance of Cd(II) and Pb(II) ions on both unmodified MCM-41 and amine-functionalized MCM-41 samples. The data reveal that pure MCM-41 exhibits a relatively lower adsorption capacity for Cd(II) (Fig. 6a) and Pb(II) (Fig. 6b) ions compared to its amine-modified counterparts—3 mL-NH_2-MCM-41, 5 mL-NH_2-MCM-41, 8 mL-NH_2-MCM-41, and 15 mL-NH_2-MCM-41. These findings indicate that the introduction of amine groups enhances the adsorption efficiency of MCM-41.

The adsorption capacity of the material initially increases with higher amine loading, peaking at the 5 mL-NH_2-MCM-41 sample. Beyond this point, further amine functionalization results in a decline in adsorption efficiency. This reduction can be attributed to interactions between the excess amine groups and the surface silanol groups located at the entrances of the mesoporous channels or on the external surfaces of the adsorbent. Such interactions cause a dense accumulation of organic-amine moieties at the pore openings, leading to a bottleneck effect that obstructs the homogeneous distribution of functional groups within the pores.

Consequently, the effective pore size and total pore volume of amine-modified samples decrease, as confirmed by their textural properties (Table 1). The restricted pore access diminishes the likelihood of Cd(II) and Pb(II) ions interacting with amine groups situated inside the mesopores. Similar adsorption behavior has been reported by Xia et al. [44]. Additionally, increased amine loading can lead to a localized concentration of amine functional groups, which facilitates interactions among adjacent amine molecules via hydrogen bonding, thereby reducing their overall reactivity and adsorption efficiency [45].

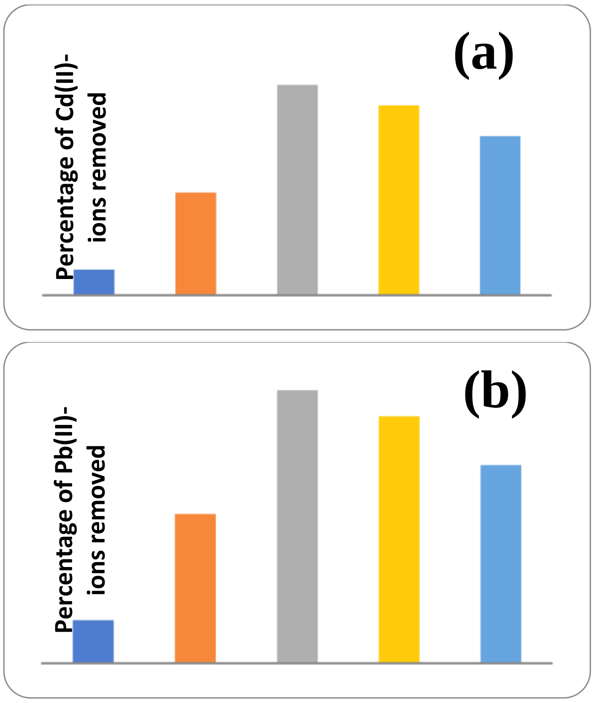

Figure 6. Comparative Ion Removal Efficiency Across Different Adsorbents Evaluation of Cd(II) and Pb(II) removal percentages using pure MCM-41 and amine-functionalized MCM-41 variants (3 mL-NH_2-MCM-41, 5 mL-NH_2-MCM-41, 8 mL-NH_2-MCM-41, and 15 mL-NH_2-MCM-41).

The 5 mL-NH_2-MCM-41 sample exhibited the highest adsorption capacity for both Cd(II) and Pb(II) ions, making it the most effective adsorbent among the tested materials. Consequently, this sample was chosen for further experimentation throughout the study.

2.3. Influence of Solution pH on Cd(II) and Pb(II) Adsorption by 5 mL-NH_2-MCM-41

The pH of the solution plays a crucial role in determining the solubility, speciation, and adsorption behavior of heavy metal ions. Changes in pH influence the ionization and chemical speciation of pollutants, thereby affecting the reaction kinetics and equilibrium of the adsorption process [46]. Figure 7 presents the adsorption data for Cd(II) and Pb(II) ions, demonstrating that adsorption efficiency increases as pH rises, reaching maximum adsorption rates of 89.7% at pH 5.5 for Cd(II) and 95.3% at pH 3.0 for Pb(II).

At lower pH levels, a high concentration of hydronium ions (H_3O^+) competes with Cd(II) and Pb(II) ions for adsorption sites, reducing the effectiveness of metal ion binding [47]. Furthermore, the oxygen atoms on the surface of MCM-41 may interact with water molecules, forming positively charged aqua-complexes [47], which repel Cd(II) and Pb(II) ions, further hindering adsorption. As the pH increases, proton concentrations decrease, rendering the adsorbent surface more negatively charged and making adsorption sites more accessible for metal ions.

However, at elevated pH levels, Pb(II) ion adsorption declines due to the formation of insoluble hydroxylated complexes, such as lead hydroxide ($Pb(OH)_2$) [48]. Based on these findings, pH values of 3 and 5.5 were identified as the optimal conditions for Pb(II) and Cd(II) adsorption, respectively, and were applied in subsequent experiments.

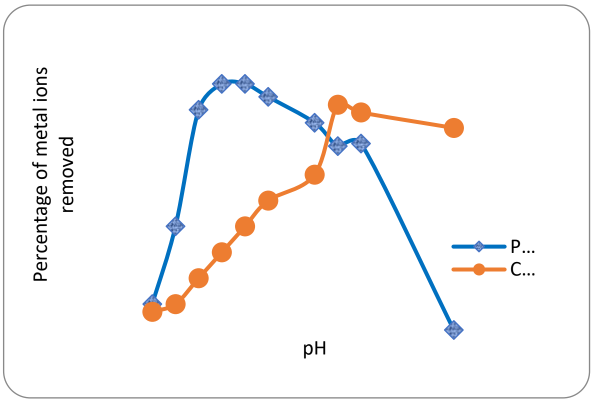

Figure 7. Influence of Solution pH on the Adsorption Efficiency of Cd(II) and Pb(II) Using 5 mL-NH_2-MCM-41 Experimental conditions: Initial metal ion concentration of 30 ppm; adsorbent dosage of 0.1 g; contact time of 2 hours; agitation speed maintained at 250 strokes per minute; ambient temperature controlled at 20 ± 2 ºC.

2.4. Influence of 5 mL-NH_2-MCM-41 Adsorbent Dosage on Cd(II) and Pb(II) Ion Adsorption

The effect of varying the dosage of 5 mL-NH_2-MCM-41 on Cd(II) and Pb(II) adsorption was examined by adjusting the amount of adsorbent from 0.25 g to 3.0 g, maintaining an initial metal ion concentration of 30 ppm. These adsorption experiments were conducted at pH 5.5 for Cd(II) ions and pH 3.0 for Pb(II) ions, with the results illustrated in Fig. 8.

An increase in adsorbent dosage from 0.25 to 3.0 g enhanced Cd(II) adsorption from 84% to 89%, while Pb(II) adsorption rose from 88.5% to 95% within the same dosage range. The findings indicate that adsorption capacity improves with higher dosages of amine-functionalized MCM-41, attributed to the greater availability of active binding sites, which facilitate the interaction and complexation of metal ions [49].

For both Cd(II) and Pb(II), the adsorption rate initially increases sharply with increasing adsorbent quantity. However, beyond a certain threshold, the rate of adsorption begins to level off—reaching a saturation point at approximately 1.5 g for Pb(II) and 2.0 g for Cd(II). Notably, Pb(II) ions demonstrate a higher adsorption efficiency than Cd(II) under identical experimental conditions.

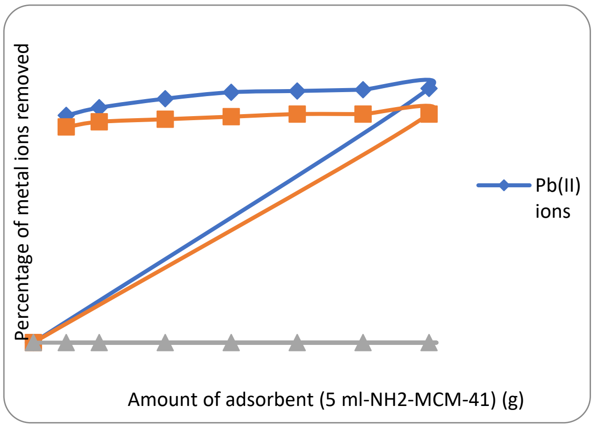

Figure 8. Influence of Adsorbent Dosage on Cd(II) and Pb(II) Ion Removal Using 5 mL-NH_2-MCM-41 Experimental conditions: Initial metal ion concentration of 30 ppm; pH values set at 5.5 for Cd(II) and 3.0 for Pb(II); agitation speed maintained at 250 strokes per minute; contact time of 2 hours; ambient temperature controlled at 20 ± 2 ºC.

2.5. Influence of Initial Cd(II) and Pb(II) Ion Concentration on Adsorption by 5 mL-NH_2-MCM-41

The impact of varying initial concentrations of Cd(II) and Pb(II) ions on adsorption was examined, with the findings illustrated in Figure 9. The results indicate that adsorption efficiency remained relatively stable for both Cd(II) and Pb(II) ions up to a concentration of 30 ppm. However, beyond this threshold, a noticeable decline in adsorption capacity was observed. This trend suggests that at concentrations exceeding 30 ppm, the available adsorption sites become saturated, limiting further uptake of metal ions by the adsorbent.

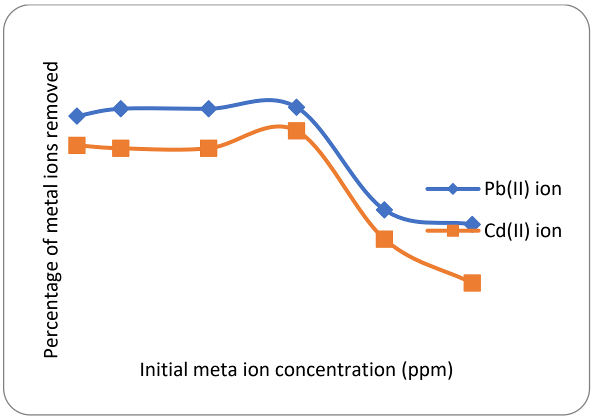

Figure 9. Influence of Initial Cd(II) and Pb(II) Concentration on Adsorption Efficiency of 5 mL-NH_2-MCM-41 Adsorption conditions: pH values of 5.5 for Cd(II) and 3.0 for Pb(II); agitation speed set at 250 strokes per minute; adsorbent dosage of 0.1 g; contact time of 2 hours; ambient temperature maintained at 20 ± 2 ºC.

2.6 Influence of Temperature on Adsorption by 5 mL-NH_2-MCM-41

The effect of temperature on the percentage removal of Cd(II) and Pb(II) ions using 5 mL-NH_2-MCM-41 was analyzed, with the findings displayed in Fig. 10. The results demonstrate that as the temperature increases from 20°C to 40°C, the adsorption efficiency significantly improves, rising from 30% to 80% for Cd(II) and from 34.5% to 88.5% for Pb(II). This observed enhancement in adsorption capacity at higher temperatures is likely due to an improved equilibrium effect.

While the interaction between amine groups and metal ions is an exothermic process, the diffusion of heavy metal ions into the adsorbent's pores is endothermic. The resulting positive enthalpy change from the diffusion process may outweigh the negative enthalpy associated with complex formation between the metal ions and amine groups, leading to an overall positive enthalpy effect [50]. Consequently, increasing the temperature facilitates the adsorption process, making it more effective for Cd(II) and Pb(II) ion uptake onto the 5 mL-NH_2-MCM-41 adsorbent.

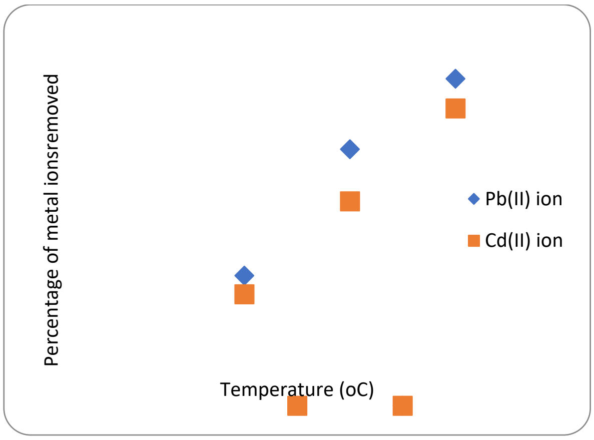

Figure 10. Influence of Temperature on Cd(II) and Pb(II) Adsorption Behavior Experimental conditions: Initial metal ion concentration of 30 ppm; pH values of 5.5 for Cd(II) and 3.0 for Pb(II); agitation speed of 250 strokes per minute; contact time of 2 hours.

2.8. Adsorption Isotherms

Figures 11 and 12 illustrate the experimental data modeled using both Langmuir and Freundlich isotherms. When applying the Langmuir model, the R-squared values obtained were 0.991 for Cd(II) (Fig. 11a) and 0.998 for Pb(II) (Fig. 11b), indicating a strong correlation. In contrast, the Freundlich model yielded R-squared values of 0.947 for Cd(II) (Fig. 12a) and 0.983 for Pb(II) (Fig. 12b). These results suggest that the Langmuir isotherm provided the best fit for the experimental data.

Additionally, the separation factor RLR_L, a dimensionless parameter derived from Langmuir isotherm constants, was calculated using Equation 5. The values were determined to be 0.049 for Cd(II) and 0.059 for Pb(II), further supporting the adsorption characteristics observed in this study.

$$R_L = \frac{1}{1+bC_0} \tag{5}$$

The parameter **b** (mg/L) represents the Langmuir adsorption constant, while **C_0** denotes the optimal initial metal ion concentration (mg/L). Table 3 summarizes the values of all fitted parameters obtained from the Langmuir isotherm model. Studies have consistently reported that **RL** values ranging between 0 and 1 indicate a favorable adsorption process [51-53].

In this study, the calculated RL values for Cd(II) and Pb(II) ions were 0.049 and 0.059, respectively, confirming that the adsorption of these metal ions onto the amine-functionalized MCM-41 mesoporous sample was favorable. Generally, the RL value provides insight into the nature of adsorption: **RL > 1** indicates an unfavorable process, **RL = 1** suggests linear adsorption behavior, **0 < RL < 1** signifies a favorable adsorption interaction, and **RL = 0** represents irreversible adsorption [54].

Furthermore, the Langmuir isotherm model reveals that the adsorption capacity of Cd(II) ions is greater than that of Pb(II) ions, suggesting that Cd(II) exhibits stronger adsorption energy in comparison to Pb(II).

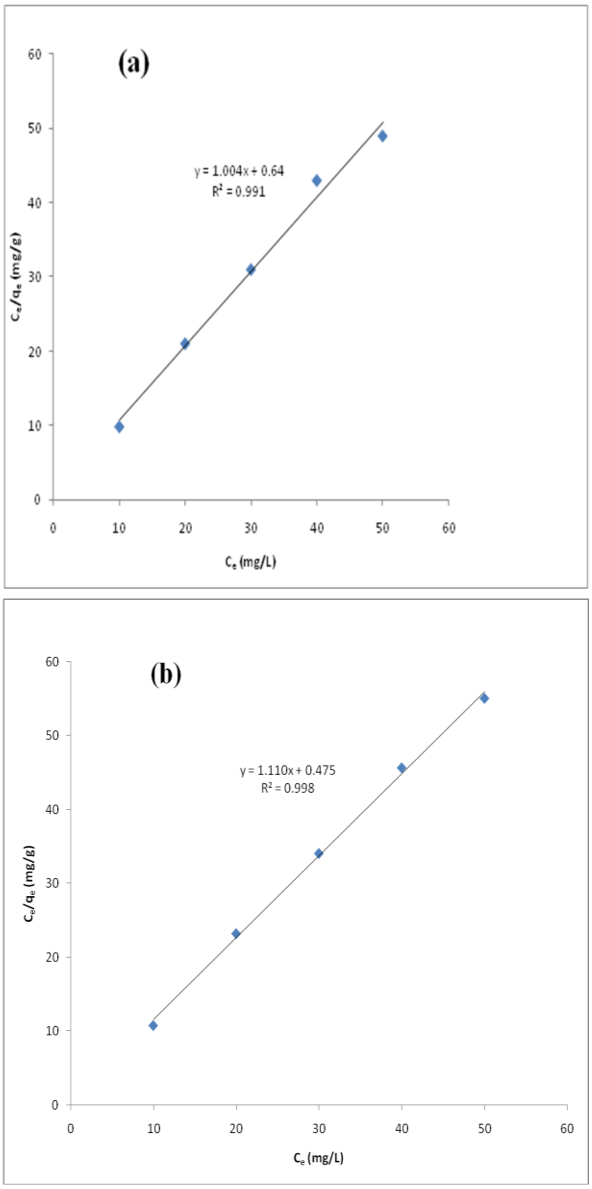

Figure 11. Langmuir Isotherm Model Fitting for Adsorption Studies (a) Cd(II) adsorption profile and (b) Pb(II) adsorption profile.

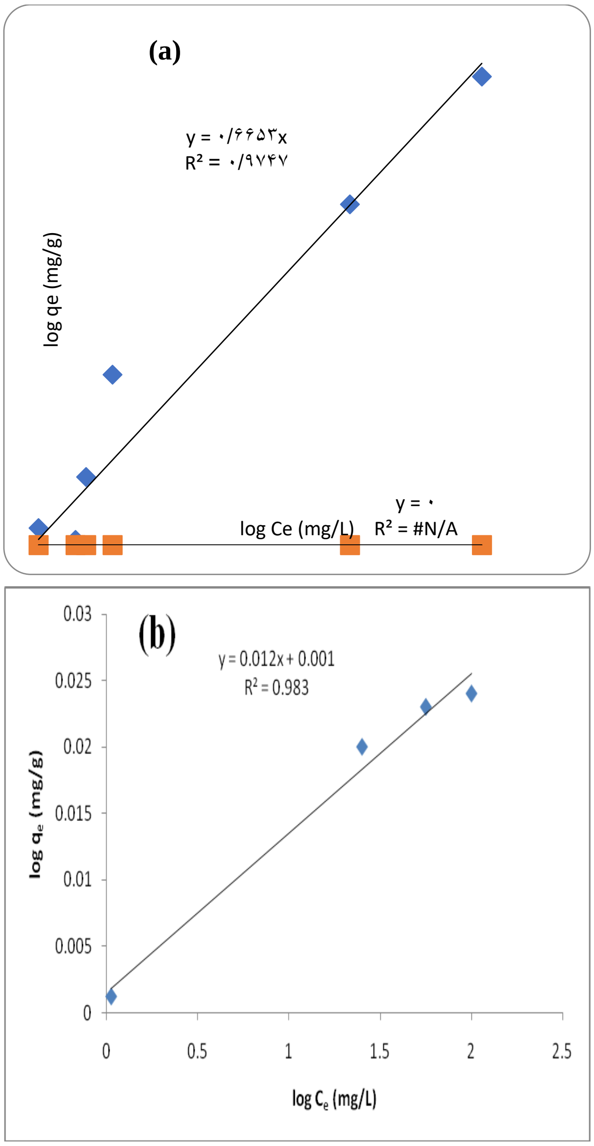

Figure 12. Adsorption Data Fitted to the Freundlich Isotherm Model for Metal Ion Removal (a) Cd(II) adsorption profile and (b) Pb(II) adsorption profile.

Table 3. Isotherm Model Parameters and Correlation Coefficients for Cd(II) and Pb(II) Adsorption onto 5 mL-NH$_2$-MCM-41

Heavy metal ion	Langmuir			
	$q_{max}(mg/g)$	b	R_L	R^2
Cd(II) ion	55.1	0.643	0.049	0.991
Pb(II) ion	49.0	0.528	0.059	0.998

2.9. Adsorption Kinetics

Kinetic analyses were performed on mesoporous silica adsorbents modified with APTES, with 5 mL-NH$_2$-MCM-41 chosen as the representative material to assess adsorption characteristics across comparable systems. The study aimed to elucidate mass transfer mechanisms and the reaction kinetics governing the uptake of metal ions onto 5 mL-NH_2-MCM-41.

To analyze the adsorption kinetics, the first-order and second-order models introduced by Lagergren [55] and Ho & McKay [56] were applied. Specifically, the pseudo-first-order kinetic model, as described by Lagergren et al., was used and is mathematically expressed in equation (6).

$$\log(q_e - q_t) = \log q_e - \frac{K_{ad}}{2.303}t \tag{6}$$

In this context, $\mathbf{q_e}$ and $\mathbf{q_t}$ denote the quantities of Cd(II) or Pb(II) ions (mg/L) adsorbed at equilibrium and at a given time **t**, respectively. The parameter $\mathbf{K_ad}$ represents the first-order adsorption equilibrium constant. To determine this constant and assess adsorption behavior, linear plots of $\mathbf{log(q_e - q_t)}$ versus **t** were analyzed for various concentrations.

However, the correlation coefficients ($\mathbf{R^2}$) obtained from these plots were relatively low, as shown in Figure 13a for Cd(II). These weak correlations suggest that the adsorption process for Cd(II) and Pb(II) ions onto the amine-modified mesoporous adsorbent does not conform to first-order kinetics.

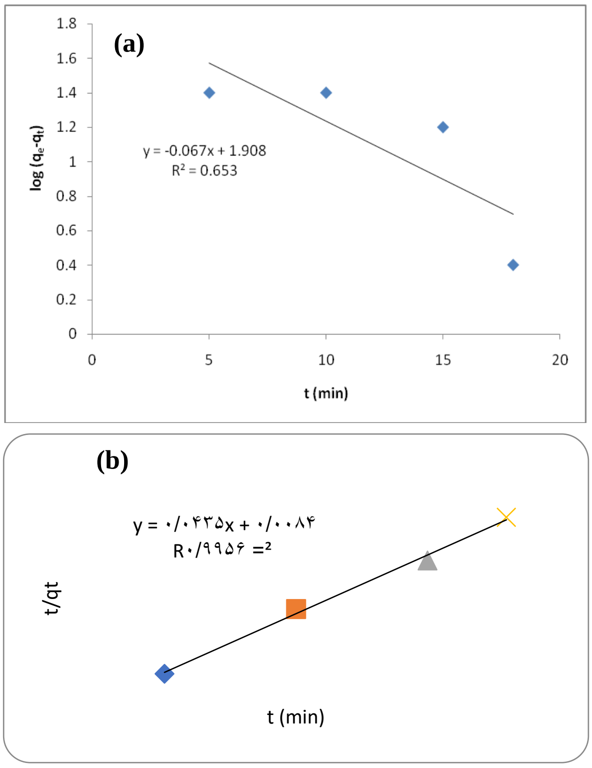

Figure 13. (a) Kinetic model of pseudo-first-order for Cd(II) adsorption (30 ppm) onto 5 mL-NH_2-MCM-41 and (b) pseudo-second-order kinetic plot illustrating Pb(II) adsorption on 5 mL-NH_2-MCM-41. Experimental conditions: pH 3.0 for Pb(II), pH 5.5 for Cd(II); agitation speed of 250 strokes per minute; contact time of 2 hours at an ambient temperature of 20 ± 2 ºC.

2.10. Pseudo-Second-Order Kinetics

The adsorption process was further analyzed using the pseudo-second-order kinetic model, which is mathematically represented as equation (7). Here, **h** denotes the initial adsorption rate (mg/g min), while **k** (g/mg min) is the second-order rate constant of adsorption. If adsorption follows second-order kinetics, a plot of $\mathbf{t/q_t}$ versus **t** should exhibit a linear trend.

Figure 13b presents the model fitting for second-order kinetics. The obtained correlation coefficients ($\mathbf{R^2}$) of 0.987 for Cd(II) and 0.995 for Pb(II) suggest a strong linear relationship, indicating that the adsorption process predominantly follows second-order kinetics. The high correlation values confirm that this model provides a significantly better representation of Cd(II) and Pb(II) adsorption onto 5 mL-NH_2-MCM-41. This suggests that both external and internal mass transfer mechanisms are involved in the adsorption process [57].

2.11. Desorption and Regeneration Studies

The reusability of an adsorbent is a key consideration for practical applications. Therefore, desorption and regeneration experiments were conducted to evaluate the reversibility of Cd(II) and Pb(II) adsorption onto 5 mL-NH_2-MCM-41. The desorption efficiency was assessed using HCl solutions at concentrations of 0.2 M, 0.5 M, and 0.75 M. Among these, the 0.5 M HCl solution demonstrated the highest efficiency, successfully desorbing approximately **0.083 g/L** of Pb(II), corresponding to a desorption rate of about **80%**. The desorption efficiency increased as the concentration of the eluent was raised.

After desorption, the adsorbents were air-dried at room temperature before being reused for further metal ion adsorption. To evaluate the material's long-term usability, the adsorbent was subjected to **four adsorption–desorption cycles**. Figure 13 illustrates that after four cycles, Cd(II) removal efficiency remained above **85%**, while Pb(II) removal remained above **90%**. These results confirm the excellent regeneration capability of the 5 mL-NH_2-MCM-41 adsorbent material. After each cycle, the used adsorbent was thoroughly washed with distilled water before reuse.

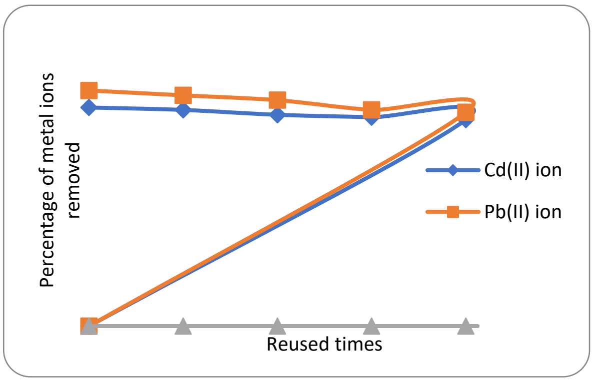

Figure 14. Removal efficiency of Cd(II) and Pb(II) ions using 5 mL-NH_2-MCM-41 across multiple adsorption cycles. (Initial metal ion concentration: 30 ppm; pH conditions: 5.5 for Cd(II) and 3.0 for Pb(II); agitation speed: 250 rpm; contact time: 2 hours; ambient temperature: 25 ± 2 ºC)

2.12. Comparative Analysis of Sorbents

The $\mathbf{q_e}$ value and adsorption percentage serve as key indicators in determining the sorbent with the highest adsorption capacity. Table 4 presents a comparative assessment of adsorption performance, highlighting the adsorption capacity and efficiency of various sorbents documented in previous studies in relation to the present sorbent system.

Table 4. Comparative Analysis of Cd(II) and Pb(II) Adsorption Capacity and Removal Efficiency Across Different Adsorbents

Metal ion	Adsorbent	% Removal	Reference
Cd^{2+}	Monoamine-functionalized silica and activated silica	78.0	[58]
Cd^{2+}	NH_2-MCM-41	93	[59]
Cd^{2+}	Radish Peels	88.2	[6]
Pb^{2+}	Amino-functionalized ordered-mesoporous silica	80	[60]
Pb^{2+}	Radish Peels	85.6	[6]
Pb^{2+}	Ethylenediamine-functionalized SBA-15	98.5	[3]
Cd^{2+}	Amine-functionalized MCM-41	89.1	This study
Pb^{2+}	Amine-functionalized MCM-41	95.3	This study

3. Conclusions

Amine-functionalized MCM-41, a hybrid organic-inorganic material, exhibited high adsorption efficiency for Cd(II) and Pb(II) ions in aqueous environments. Among the synthesized samples, 5 wt% NH2-MCM-41 demonstrated superior adsorption capacity for Pb(II) compared to Cd(II) under identical conditions. Compared to unmodified MCM-41, the amine-functionalized variants showed significantly enhanced performance, attributed to strong coordination and electrostatic interactions between amine groups and metal ions.

Adsorption studies identified optimal pH ranges of 5.0–6.0 for Cd(II) and 3.0–3.5 for Pb(II) removal, highlighting the pH dependence of adsorption behavior. Adsorption equilibrium was reached within 60 minutes, indicating rapid metal ion uptake. The adsorption isotherms correlated strongly with the Langmuir model, while kinetic analysis confirmed that the process followed the pseudo-second-order model.

In summary, the amine-functionalized MCM-41 adsorbent demonstrated high efficiency in removing Cd(II) and Pb(II) from aqueous solutions. Its advantages include high adsorption capacity, rapid kinetics, and excellent reusability, with structural integrity maintained over multiple adsorption-regeneration cycles, making it a promising candidate for water treatment applications. Under optimized conditions, the adsorbent performed competitively with other reported materials in terms of efficiency and uptake rate. Given its properties, amine-functionalized mesoporous silica holds strong potential for large-scale heavy metal ion removal in water purification and wastewater treatment.

Conflict of Interest

There are no conflicts to declare.

Acknowledgements

We acknowledge the Imam Khomeini International University for support of this work.

References

1. V.H. Morales, R. Nava, Y.J.A. Silva, S.A.M. Sánchez, J.J.P. Bueno, B. Pawelec, Micropor. Mesopor. Mater. 160, 133 (2012). DOI: https://doi.org/10.1016/j.micromeso.2012.04.032
2. M. R. Mehrasbi, Z. Farahmandkia, B. Taghibeigloo, A. Taromi, Water Air Soil Pollut. 199, 343 (2009). DOI: https://doi.org/10.1007/s11270-008-9875-8
3. L. Hajiaghababaei, A. Badiei, M.R. Ganjali, S. Heydari, Y. Khaniani, G.M. Ziarani, Desalination 266, 182

(2011). DOI: https://doi.org/10.1016/j.desal.2010.08.020
4. A. Sari, D. Mendil, M. Tuzen, M. Soylak, Chem. Eng. J. 144, 1 (2008). DOI: https://doi.org/10.1016/j.cej.2007.12.005
5. O.M.M. Freitas, R.J.E. Martins, C.M. Delerue-Matos, R.A.R. Boaventura, J. Hazard. Mater. 153, 493 (2008). DOI: https://doi.org/10.1016/j.jhazmat.2007.08.083
6. J. Anwar, U. Shafique, M.S. Waheed-uz Zaman, M. Memoona, J. Sci. Res. XXIX, 29 (2009).
7. A.T. Paulino, L.B. Santos, J. Nozaki, React. Funct. Polym. 68, 634 (2008). DOI: https://doi.org/10.1016/j.reactfunctpolym.2007.10.003
8. R. Naseem, S.S. Tahir, Water Res. 35, 3982 (2001). DOI: https://doi.org/10.1016/S0043-1354(01)00113-9
9. M.A. Hasan, Y.T. Selim, K.M. Mohamed, J. Hazard. Mater. 168, 1537 (2009). DOI: https://doi.org/10.1016/j.jhazmat.2009.03.024
10. T.S. Huuha, T.A. Kurniawan, M.E.T. Sillanpää, Chem. Eng. J. 158, 584 (2010). DOI: https://doi.org/10.1016/j.cej.2010.02.001
11. W. Plazinski, W. Rudzinski, Environ Sci. Technol. 43, 7465 (2009). DOI: https://doi.org/10.1021/es901956a
12. R. Rostamian, M. Najafi, A.A. Rafati, Chem. Eng. J. 171, 1004 (2011). DOI: https://doi.org/10.1016/j.cej.2011.04.034
13. K.K. Singh, M. Talat, S.H. Hasan, Bioresource Technology 97, 2124 (2006). DOI: 10.1016/j.biortech.2005.09.016
14. J. Aguado, J.M. Arsuaga, A. Arencibia, M. Lindo, V. Gascón, Journal of Hazardous Materials 163, 213 (2009). DOI: https://doi.org/10.1016/j.jhazmat.2008.06.080
15. C. McManamon, A.M. Burke, J.D. Holmes, M.A. Morris, Journal of Colloid and Interface Science 369, 330 (2012). DOI: https://doi.org/10.1016/j.jcis.2011.11.063
16. S. Li, X. Yue, Y. Jing, S. Bai, Z. Dai, Colloids and Surfaces A: Physicochemical and Engineering Aspects 380, 229 (2011). DOI: https://doi.org/10.1016/j.colsurfa.2011.02.044
17. A. Ely, M. Baudu, M.O.S.A.O. Kankou, J. Basly, Chemical Engineering Journal 178, 168 (2011). DOI: https://doi.org/10.1016/j.cej.2011.10.040
18. V.K. Jha, M. Matsuda, M. Miyake, Journal of Hazardous Materials 160, 148 (2008). DOI: https://doi.org/10.1016/j.jhazmat.2008.02.107
19. D. Zhang, C. Zhang, P. Zhou, Journal of Hazardous Materials 186, 971 (2011). DOI: https://doi.org/10.1016/j.jhazmat.2010.11.096
20. D. Vu, Z. Li, H. Zhang, W. Wang, Z. Wang, X. Xu, B. Dong, C. Wang, Journal of Colloid and Interface Science 367, 429 (2012). DOI: https://doi.org/10.1016/j.jcis.2011.09.088
21. J. Wang, L. Xua, Y. Meng, C. Cheng, A. Li, Chem. Eng. J. 178, 108 (2011) DOI: https://doi.org/10.1016/j.cej.2010.11.016
22. L. Wang, Z. Huang, M. Zhang, B. Chai, Chem. Eng. J. 189-190, 168 (2012) DOI: https://doi.org/10.1016/j.cej.2012.02.015
23. X. Feng, G.E. Fryxell, L.Q. Wang, A.Y. Kim, J. Liu, K.M. Kemner, Science 276, 923 (1997) DOI: 10.1126/science.276.5314.923
24. A. Sayari, S. Hamoudi, Chem. Mater. 13, 3151 (2001) DOI: https://doi.org/10.1021/cm011039l
25. C.T. Kresge, M.E. Leonowicz, W.J. Roth, J.C. Vartuli, J.S. Beck, Nature 359, 710 (1992) DOI: https://doi.org/10.1038/359710a0
26. P.T. Tanev, T.J. Pinnavaia, Science 267, 865 (1995) DOI: https://doi.org/10.1126/science.267.5199.865
27. A. Vinu, K.Z. Hossain, K. Ariga, J. Nanosci. Nanotechnol. 5, 347 (2005) DOI: https://doi.org/10.1166/jnn.2005.089347
28. E. Da'na, A. Sayari, Chem. Eng. J. 166, 445 (2011) DOI: https://doi.org/10.1016/j.cej.2010.11.016
29. L. Mercer, T.J. Pinnavaia, Environ. Sci. Technol. 32, 2749 (1998) DOI: https://doi.org/10.1021/es980017n
30. U. Wingenfelder, B. Nowack, G. Furrer, R. Schulin, Water Res. 39, 3287 (2005) DOI: https://doi.org/10.1016/j.watres.2005.06.011
31. X.G. Wang, K.S.K. Lin, J.C.C. Chan, S. Cheng, J. Phys. Chem. B 109, 1763 (2005) DOI: https://doi.org/10.1021/jp045113o
32. Y. Tang, K. Landskron, J. Phys. Chem. C 114, 2494 (2010) DOI: https://doi.org/10.1021/jp908856p
33. J.W. Choi, S.Y. Lee, S.G. Chung, S.W. Hong, D.J. Kim, S.H. Lee, Water Air Soil Pollut. 222, 243 (2011) DOI: https://doi.org/10.1007/s11270-011-0762-4
34. Y. Goksungur, S. Uren, U. Guvenc, Bioresource Technol. 96, 103 (2005) DOI: https://doi.org/10.1016/j.biortech.2004.02.009
35. E.A. Mehrizi, M. Sadani, M. Karimaei, E. Ghahramani, K. Ghadiri, M.S. Taghizadeh, World Appl. Sci. J. 15, 1678 (2011) DOI: https://doi.org/10.5829/idosi.wasj.2011.15.12.331
36. E. Vunain, A.K. Mishra, R.W. Krause, J. Inorg. Organomet. Polym. 23, 293 (2013) DOI: https://doi.org/10.1007/s10904-012-9759-0
37. Y. Toshiyuki, Y. Hideaki, T. Takashi, J. Mater. Chem. 14, 951 (2004) DOI: https://doi.org/10.1039/b312794d
38. J.H. Yim, D. Kim, J.A. Bae, Y.K. Park, J.H. Park, J.K. Jeon, S.H. Park, J. Song, S.S. Kim, J. Nanosci. Nanotechnol. 11, 1714 (2011) DOI: https://doi.org/10.1166/jnn.2011.3859
39. G. Lin, S. Jihong, L. Yuzhen, J. Solid State Chem. 184, 1909 (2011) DOI: https://doi.org/10.1016/j.jssc.2011.06.011
40. P. Luigi, T. Flaviano, A. Rosario, C. Sante, B.N. Janos, Micropor. Mesopor. Mater. 103, 166 (2007) DOI: https://doi.org/10.1016/j.micromeso.2007.05.011
41. K.M. Parida, R. Dharitri, J. Molecul. Catal. A: Chemical. 310, 93 (2009) DOI: https://doi.org/10.1016/j.molcata.2009.02.001
42. L. Tongge, L. Gang, N. Zhang, C. Yongying, J. Hazard. Mater. 201-202, 155 (2012) DOI: https://doi.org/10.1016/j.jhazmat.2011.11.058
43. L.P. Mercuri, J.R. Matos, Z. Li, M. Jaroniec, J. Coll. Interf. Sci. 296, 377 (2006) DOI: https://doi.org/10.1016/j.jcis.2005.08.012
44. K. Xia, R.Z. Ferguson, M. Losier, N. Tchoukanova, R. Bruning, Y. Djaoued, J. Hazard. Mater. 183, 554 (2010) DOI: https://doi.org/10.1016/j.jhazmat.2010.07.097
45. H.W. Lee, H.J. Cho, J.H. Yim, J.M. Kim, J.K. Jeon, J.M. Sohn, K.S. Yoo, S.S. Kim, Y.K. Park, J. Ind. Eng. Chem. 17, 504 (2011) DOI: https://doi.org/10.1016/j.jiec.2010.12.003

46. B.Y.M. Bueno, M.L. Torem, F. Molina, L.M.S. De Mesquita, Minerals Eng. 21, 65 (2008) DOI: https://doi.org/10.1016/j.mineng.2007.07.005
47. M. Anbia, M. Lashgari, Chem. Eng. J. 150, 555 (2009) DOI: https://doi.org/10.1016/j.cej.2009.02.022
48. M. Azza, Aty-Abdel, N.S. Ammar, H.H.A. Ghafar, R.K. Ali, J. Adv. Res. 4, 367 (2013) DOI: https://doi.org/10.1016/j.jare.2012.09.006
49. A. Ahmada, M. Rafatullahb, O. Sulaimanb, H.M. Ibrahima, Y.Y. Chiia, B.M. Siddiquea, Desalination 247, 636 (2009) DOI: https://doi.org/10.1016/j.desal.2008.06.052
50. S. Haoa, Y. Zhong, F. Pepeb, W. Zhu, Chem. Eng. J. 189-190, 160 (2012) DOI: https://doi.org/10.1016/j.cej.2012.02.014
51. J. Zhang, S. Zhai, S. Li, Z. Xiao, Y. Song, Q. An, G. Tian, Chem. Eng. J. 215–216, 461 (2013) DOI: https://doi.org/10.1016/j.cej.2012.10.043
52. S.K. Maji, A. Pal, T. Pal, J. Hazard. Mater. 151, 811 (2008) DOI: https://doi.org/10.1016/j.jhazmat.2007.07.011
53. T.K. Naiya, A.K. Bhattacharya, S.K. Das, J. Coll. Interf. Sci. 333, 14 (2009) DOI: https://doi.org/10.1016/j.jcis.2009.02.003
54. K.Y. Foo, B.H. Hameed, J. Chem. Eng. 156, 2 (2010) DOI: https://doi.org/10.1016/j.cej.2009.11.021
55. S. Azizian, J. Coll. Interf. Sci. 276, 47 (2004) DOI: https://doi.org/10.1016/j.jcis.2004.01.006
56. Y.S. Ho, G. Mckay, Chem. Eng. J. 70, 115 (1998) DOI: https://doi.org/10.1016/S1385-8947(97)00183-6
57. M.A. Malana, S. Ijaz, M.N. Ashiq, Desalination 263, 249 (2010) DOI: https://doi.org/10.1016/j.desal.2010.06.011
58. M. Machida, B. Fotoohi, Y. Amamo, T. Ohba, H. Kanoh, L. Mercier, J. Hazard. Mater. 221-222, 220 (2012) DOI: https://doi.org/10.1016/j.jhazmat.2012.03.005
59. A. Heidari, H. Younesi, Z. Mehraban, Chem. Eng. J. 153, 70 (2009) DOI: https://doi.org/10.1016/j.cej.2009.05.008
60. A.M. Showkat, Y.P. Zhang, M.S. Kim, A.L. Gopalan, K.R. Reddy, K.P. Lee, Bull Korean Chem. Soc. 28, 1985 (2007) DOI: https://doi.org/10.5012/bkcs.2007.28.12.1985